JOURNAL OF CATALYSIS **177,** 53–59 (1998)
ARTICLE NO. CA982072

Unusual Redox Properties of Bismuth in Sol–Gel Bi-Mo-Ti Mixed Oxides

Jan-Dierk Grunwaldt, Manuel D. Wildberger, Tamas Mallat, and Alfons Baiker[1]

Laboratory of Technical Chemistry, Swiss Federal Institute of Technology, ETH-Zentrum, CH-8092 Zürich, Switzerland

Received December 4, 1997; revised March 4, 1998; accepted March 5, 1998

Novel bismuth molybdenum titanium oxide catalysts, prepared via different sol–gel routes, were studied by X-ray photoelectron spectroscopy (XPS) at ambient temperature after evacuation and after reaction with hydrogen or oxygen. The surface Bi^{3+} and Mo^{6+} species of several sol–gel catalysts could be reduced and re-oxidized at room temperature, whereas the two reference materials γ-bismuth molybdate and Bi_2O_3 were not reduced in hydrogen (10^{-4} mbar) at temperatures below 573 K. The reduction of Bi^{3+} to Bi^0 was observed to be remarkably more facile than that of Mo^{6+} to Mo^{5+}. Reduction of surface bismuth species in hydrogen and re-oxidation in oxygen could be followed by XPS at room temperature in the pressure range of 10^{-6}–10^{-4} mbar over a time scale of a few minutes to several hours. The facile reduction of surface Bi^{3+} is probably not connected to the bulk or surface composition. It is more likely due to the unique morphology of the bismuth molybdenum oxides stabilized by titania in the sol–gel materials. It emerged from XRD and Raman investigations that the mean crystallite size of Bi- and Mo-containing phases was around 3 nm, even after calcination at 773 K. XPS and thermoanalysis revealed that the particle size of the sol–gel mixed oxides was considerably larger (>10 nm), and the reduction of Bi^{3+} and its re-oxidation took place only in the topmost layer at ambient temperature.

Key Words: **bismuth molybdate; Bi-Mo-Ti oxide; sol–gel; XPS; surface reduction/oxidation.**

1. INTRODUCTION

The catalytic activity of bismuth molybdates has been intensively investigated over the past decades. Among the most important applications of this kind of oxidation catalysts are the selective oxidation and ammoxidation of propylene and the oxidative dehydrogenation of butene to butadiene (1–3).

The partial oxidation reactions over bismuth molybdates involve the reduction and re-oxidation processes of lattice Bi^{3+} and Mo^{6+} (2, 4). However, the redox properties of bismuth and molybdenum are not yet fully understood and surface studies by XPS measurements are rare (5–7). Grzybowska *et al.* (5) investigated the changes of the surface structure of different bismuth molybdate catalysts after outgassing, hydrogen treatment and interaction with propylene–oxygen mixtures. They found that molybdenum is reduced much easier than bismuth. In a recent study performed by Uchida *et al.* (7), Mo^{6+} and Bi^{3+} surface species of γ- and α-bismuth molybdate could only be reduced by Ar sputtering, and re-oxidation was observed when the sample was exposed to an oxygen jet of 10^{-6} Pa at 383 K. Also in this case, the rate of reduction of Mo^{6+} to Mo^{5+} was faster than that of Bi^{3+} to Bi^0.

Arora *et al.* (8) attributed the selectivity of bismuth containing metal oxides in methanol to formaldehyde transformation to highly crystalline metal oxide phases (e.g., bismuth molybdate). Hence, the structure of the particles seems to play an important role in the catalytic behavior of metal oxides. Moreover, Uchida *et al.* (7) found that the activation energies for re-oxidation of Mo^{5+} and Bi^0 species are quite different in γ- and α-bismuth molybdate due to the different mobilities of lattice oxygen.

Ultrafine metal oxides prepared via sol–gel techniques have attracted much interest in material science and heterogeneous catalysis (9). These new catalytic materials are expected to exhibit properties markedly different from those of conventional catalysts; e.g., the reactivity of lattice oxygen ions can be improved by decreasing the metal oxide particle size.

The aim of the present study was to investigate the surface redox properties of some novel Bi-Mo-Ti mixed oxides prepared via the sol–gel route. The unexpectedly facile reduction and re-oxidation of Bi^{3+} and Mo^{6+} species in the aerogel and xerogels is compared to the behavior of crystalline Bi_2O_3 and γ-bismuth molybdate.

2. EXPERIMENTAL

Sample Preparation

All sol–gel materials were prepared having 10 wt% nominal amount of bismuth molybdate ($Bi_2O_3 \cdot 2MoO_3$) and 90 wt% TiO_2. A solution of titanium(IV) tetraisopropoxide in isopropanol was prepared. Afterwards, the Mo and Bi precursors were introduced, together with a hydrolysant/acid (HNO_3) solution. The molybdenum and bismuth precursors are listed in Table 1. The first number of

[1] Corresponding author. E-mail: baiker@tech.chem.ethz.ch.

0021-9517/98 $25.00

TABLE 1

Preparation Procedure of Sol–Gel Materials and γ-Bi_2MoO_6

Catalyst	Type	Bi and Mo precursor	Prehydrolysis
10BiMoTiO-X	Xerogel	$Bi(NO_3)_3 \cdot 5H_2O$ and $(NH_4)_6Mo_7O_{24} \cdot 4H_2O$	No
10BiMoTiO-LT	Aerogel	$Bi(NO_3)_3 \cdot 5H_2O$ and $(NH_4)_6Mo_7O_{24} \cdot 4H_2O$	No
10BiMoTiO-XCl	Xerogel	$BiCl_3$ and $MoOCl_4$	No
10BiMoTiO-XClP	Xerogel	$BiCl_3$ and $MoOCl_4$	Yes
γ-Bi_2MoO_6	Fused	Bi_2O_3 and MoO_3	—

the catalyst abbreviation represents the nominal amount of bismuth molybdate in wt% (Bi/Mo atomic ratio = 1). Cl denotes the use of chlorine containing Bi and Mo precursors, P signifies prehydrolysis of the Mo and Bi precursors. X stands for xerogels which were obtained by removing the solvent *in vacuo* (10 kPa) at 373 K for 24 h. For the low temperature (LT) aerogel (10BiMoTiO-LT), the liquid was removed from the gel by semicontinuous extraction with supercritical CO_2 at 313 K and 24 MPa. In one case (10BiMoTiO-XClP), the $MoOCl_4$ and $BiCl_3$ precursors were prehydrolyzed prior to the addition to the Ti-alkoxide solution in order to equalize the hydrolysis level of all compounds. Finally, the catalysts were calcined in an O_2 flow at 773 K. Further details of the preparation can be found elsewhere (10).

For the preparation of γ-bismuth molybdate (γ-Bi_2MoO_6), equimolar amounts of Bi_2O_3 (Alfa, grade 1) and MoO_3 (Aldrich, >99%) were ground in a mortar and heated to 873 K for 10 h as described by Sant *et al.* (1). Bi_2O_3 was used as received.

Catalyst Characterization

X-ray diffraction patterns were recorded on a Siemens θ/θ D5000 powder X-ray diffractometer (CuK_α radiation, Ni-filter). The measured patterns were compared to JCPDS data files (11). Raman spectroscopy was carried out on a Perkin Elmer series 2000 instrument using the 1033 nm line of a Nd YAG laser with 200 mW power.

For ICP-AES analysis, 20 mg catalyst was dissolved in 1 ml HF (40%) and 3 ml HNO_3 (65%); 320 mg H_3BO_3 was added and the solution was diluted with H_2O to 50 g final weight. The measurements were carried out on an IRIS ICP-AES Spectrometer (Thermo Jarell Ash) in an inductive coupled Ar plasma chamber.

TPR profiles were obtained with an apparatus described previously (12); 280 mg of the calcined catalyst was placed into the reactor and heated in a flow of 5% hydrogen in argon at a heating rate of 10 K min^{-1}.

Thermoanalytical investigations (DSC/TG) were carried out at atmospheric pressure using a thermoanalyzer (Netzsch STA 409) which was connected to a pulse device suitable for pulse thermal analysis (PTA). This setup allowed the injection of small gas volumes (1.0 or 0.25 ml) into an argon carrier flow during the thermoanalytical experiments. The PTA experiments were carried out in isothermal mode at temperatures between 373 and 873 K. The weight change was followed by thermogravimetry. Evolving gases were monitored using a quadrupole mass spectrometer (Balzers QMG 420) which was connected to the thermoanalyzer by a heated capillary.

Surface Analytical Measurements

For surface analysis, a satellite system equipped with load lock, transfer, high pressure, preparation, and analysis chambers with XPS and ISS was set up. Powder samples were outgassed at room temperature till 10^{-7} to 10^{-6} mbar in the load lock. The base pressure of the transfer, preparation and analysis chambers was lower than 5×10^{-10} mbar. Additionally, the material powders could be heated up to 873 K in the reactor, preparation, and analysis chamber. In the reactor, samples could be treated with gases in a pressure range of 10^{-6} mbar to 10 bar. After treatment and evacuation in the reactor, the samples could be quickly transferred to the analysis chamber via the transfer chamber which served as a second evacuation unit. In the analysis chamber, X-ray photoelectron spectroscopic analysis was performed on a Leybold Heraeus LHS 11 MCD instrument at a pressure of 10^{-9} to 3×10^{-9} mbar with Mg K_α radiation (12 kV, 20 A). Photoelectrons were detected by a hemispherical analyzer with 150 eV constant pass energy (for high resolution spectra at a pass energy of 37.8 eV). The binding energy scale was calibrated versus the Au $4f_{7/2}$ line at 84.0 eV and the Cu $2p_{3/2}$ line at 932.4 eV. To eliminate the steady state charging effect, corrections of the energy shift were accomplished taking the C 1s line resulting from adsorbed hydrocarbons at 285.0 eV. The surface composition of the catalysts was determined from the areas of the Mo 3d, Bi 4f, O 1s, Ti 2p, and C 1s peaks. First, the Shirley-type background was subtracted. Second, a fitting procedure using a mixed Gauss–Lorentzian function was applied at the different binding energies in order to determine contributions from all species. Finally, the computed peak areas were weighted with empirically derived cross section factors for XPS (13, 14).

For time-resolved reduction and re-oxidation of the surfaces, the following procedure was applied: The sample was introduced into the reactor and treated for a definite time (2 min to 20 h) in hydrogen or oxygen at a partial pressure of 10^{-6}–10^{-4} mbar. After quick evacuation ($t < 30$ s, $p < 5 \times 10^{-8}$ mbar) the sample was transferred via the transfer chamber ($p < 10^{-9}$ mbar) into the analysis chamber where the XPS analysis was performed. The amount of reduced Bi was calculated by computing the peak areas of the four Bi^{3+} and Bi^0 peaks.

3. RESULTS

Structure and Composition of the Materials

The bulk and surface composition of various Bi- and Mo-containing catalysts, determined by XRD, ICP-AES, and XPS analysis, are summarized in Table 2. In the calcined bismuth molybdenum titanium mixed oxides, only XRD-reflections related to anatase were detected. The anatase crystallites had a mean diameter of ca 15 nm. The bismuth molybdenum oxide phases were X-ray amorphous in all sol–gel derived materials even after calcination at 773 K, which indicates that there were no crystalline parts present or the crystallites were smaller than ca 3 nm. The reference sample γ-Bi_2MoO_6 exhibited a distinct XRD spectrum corresponding to γ-bismuth molybdate (11) with a mean crystallite size of 210 nm; no further phase could be detected.

Despite of the excellent sensitivity of Raman spectroscopy for the Mo-band in diluted systems (15), none of the Raman spectra of the sol–gel materials possessed a band around 900 cm^{-1} (10) which would indicate molybdenum oxide or a bismuth molybdate phase (6). We only found typical bands for anatase at 400, 525, and 635 cm^{-1} and a broad unstructured band between 700 and 950 cm^{-1} which could be due to very small bismuth molybdenum oxide particles. This is an indication that the bismuth molybdenum oxide particles are strongly stabilized in their X-ray amorphous structure in the xerogel and aerogel matrix despite the calcination at high temperatures.

Table 2 shows that the bulk Mo/Bi ratio of the sol–gel samples was unity (as designed), except when $BiCl_3$ and $MoOCl_4$ were used as precursors. The loss of Bi in the latter materials occurred during the drying and calcination steps and was assumed to be due to incomplete hydrolysis of the precursor (10). The surface Mo/Bi ratio varied in a broad range in the materials. Compared to the bulk composition, the catalysts with chloride precursors showed a bismuth surface enrichment (except after prehydrolysis), whereas the use of conventional precursors led to a molybdenum surface enrichment. The bulk and surface compositions of γ-Bi_2MoO_6 were almost identical.

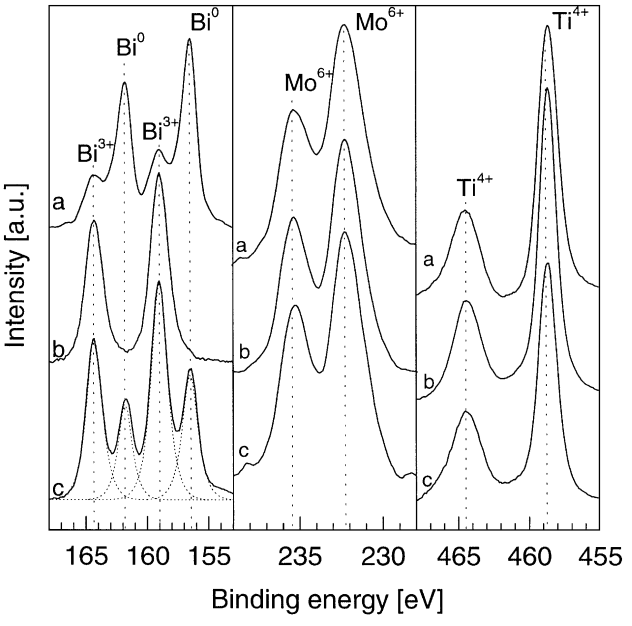

FIG. 1. High resolution XP-spectra of 10BiMoTiO-LT (a), 10BiMoTiO-XClP (b), and 10BiMoTiO-XCl (c) in the Bi 4f, the Mo 3d and the Ti 2p regions after outgassing (12 h at room temperature) in the load lock. The binding energy values are collected in Table 3.

Binding Energies and Identification of Different Surface Species by XPS

Figure 1 depicts typical high-resolution XP-spectra of three sol–gel derived mixed oxides. The spectra were obtained after outgassing the materials in the load lock for 12 h (room temperature). The position of the Ti 2p and the Mo 3d core levels, which were similar for all sol–gel derived catalysts and are listed in Table 3, are in good agreement

TABLE 2

Bulk and Surface Properties of Sol–Gel Materials and γ-Bi_2MoO_6

Catalyst	Crystalline phases (mean crystallite size in nm)	Mo/Bi_b [a] [at/at]	Mo/Bi_s [b] [at/at]	Bi^{3+} [c] [%]
10BiMoTiO-X	Anatase (13)	1.0	3.7	73
10BiMoTiO-LT	Anatase (8)	1.0	1.9	37
10BiMoTiO-XCl	Anatase (13)	1.9	0.4	65
10BiMoTiO-XClP	Anatase (11)	2.2	1.3	100
γ-Bi_2MoO_6	Bi_2MoO_6 (210)	0.5	0.6	100

[a] Bulk Mo/Bi ratio determined by ICP-AES.

[b] Surface Mo/Bi ratio determined by XPS, outgassing at ambient temperature.

[c] Percentage of surface Bi present as Bi^{3+} after outgassing for 12 h in the load lock (room temperature).

TABLE 3

Binding Energy Values Resulting from XPS Investigations

		Sol–gel materials	γ-BiMoO	Bi_2O_3
Bi^{3+}	Bi $4f_{5/2}$	164.3	164.4	163.8
	Bi $4f_{7/2}$	159.0	159.1	158.5
Bi^0	Bi $4f_{5/2}$	161.8	—	—
	Bi $4f_{7/2}$	156.4	—	—
Mo^{6+}	Mo $3d_{3/2}$	232.3	232.4	—
	Mo $3d_{5/2}$	235.5	235.5	—
Ti^{4+}	Ti $2p_{1/2}$	458.7	—	—
	Ti $2p_{3/2}$	464.5	—	—
C	C 1s	285.0	285.0	285.0
O	O 1s	529.9	530.2	529.6

with those published for Ti^{4+} (16, 17) and Mo^{6+} (18, 19). Only small shoulders on the lower binding energy side of the Mo 3d spectra were recorded. However, in the case of bismuth, some of the sol–gel derived materials showed two different bismuth species located at 159.0 eV (Bi $4f_{7/2}$) and 164.3 eV (Bi $4f_{5/2}$) as well as at 156.4 eV (Bi $4f_{7/2}$) and 161.8 eV (Bi $4f_{5/2}$), which are characteristic for Bi^{3+} and Bi^0, respectively (20–22). This surface reduction is due to the reducing conditions in the load lock (reducing gases in the zeolite trap, hydrogen from the ionization gauge, or pump oil vapor) as discussed in a later part of the paper. The possible influence of charging effects due to inhomogeneities in the samples could be excluded because the same spectrum with a higher binding energy shift was obtained when applying a tubular voltage to the analyzer.

The binding energies of Bi_2O_3 and γ-Bi_2MoO_6 are also listed in Table 3. The positions of the Bi 4f core levels are slightly shifted to lower binding energies in the case of Bi_2O_3 which is in accordance with the literature (20–22). Interestingly, the binding energies of γ-Bi_2MoO_6 are similar to those measured for the sol–gel derived samples.

In all sol–gel samples, the surface carbon content was in the range of 7.5–9.5 at% which was similar to that found in conventionally prepared materials and much lower than that of the uncalcined sol–gel materials (>20%). The C 1s peak could be deconvoluted in peaks located at 285.0 eV (C–H), 286.4 eV (C–O) and 289.2 eV (C=O). However, the contribution at 286.4 and 289.2 eV, which could stem from alkoxide residues, was very low. The predominant part of the C 1s peak at 285.0 eV probably stemmed from hydrocarbons (pump oil). Hence, we can assume that the major part of the organic residues originating from the sol–gel preparation was burnt off during calcination at 773 K in O_2. This conclusion was confirmed by thermoanalytical measurements (10).

Stability of Surface Bi^{3+} and Mo^{6+} Species in Sol–Gel Derived Materials

As summarized in the last column of Table 2, all of the sol–gel derived mixed oxides, except the prehydrolyzed sample 10BiMoTiO-XClP, showed a reduction of Bi^{3+} to Bi^0 at room temperature after evacuation in the load lock due to the reducing conditions. The presence of Bi^0 in the sol–gel samples cannot be traced to the preparation method because the samples were calcined at 773 K in oxygen before introducing them into the UHV system. Moreover, the extent of reduction is strongly dependent on the outgassing time in the load lock as illustrated in Fig. 2. After an outgassing time of $2\frac{1}{2}$ h (at room temperature), only a small amount of Bi^0 was detectable at 156.4 and 161.8 eV. After 12 h under the same conditions, most of the surface Bi^{3+} was reduced indicating that the reduction process occurred at room temperature in the load lock. Figure 2 also demonstrates that the reduced surface layer of the aerogel could easily be re-oxidized at room temperature by exposing the sample to air.

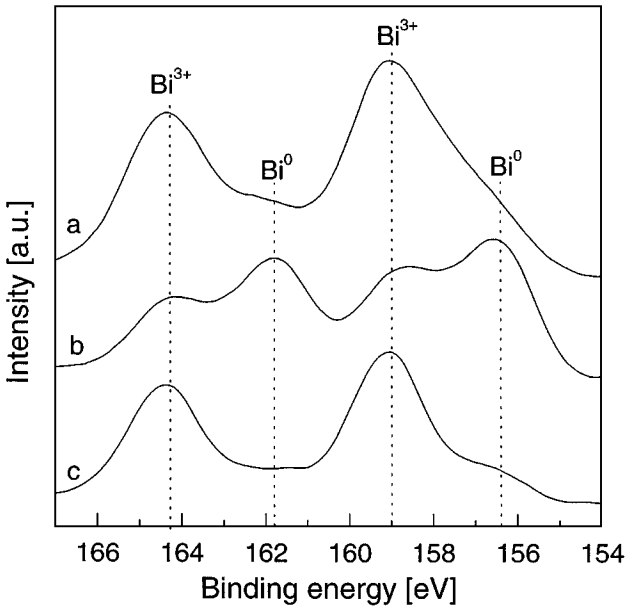

FIG. 2. High resolution XP-spectra of 10BiMoTiO-LT in the Bi 4f region after outgassing for $2\frac{1}{2}$ h (a), after outgassing for 12 h (b) and after re-oxidation in air for 2 h (c). The binding energy values are given in Table 3. Outgassing and re-oxidation were carried out at room temperature.

Investigations under UHV ($p < 10^{-9}$ mbar) and under X-ray radiation revealed that the samples were stable under these conditions and no reduction was observed. As concerns the stability of Bi^{3+} and Mo^{6+} in the sol–gel samples under UHV conditions, their behavior is similar to those of Bi_2O_3, MoO_3, and bismuth molybdates (23, 24). Hence, the samples can be handled under UHV-conditions without any chemical change on the surface. This observation will be used later for studying the dynamic behavior of the surface redox processes.

Considering the oxidation state of Mo 3d in XPS, only a small shoulder on the low binding energy side of the Mo 3d peaks could be detected in all cases. Three typical examples are shown in Fig. 1. A peak fitting procedure with Mo species at 232.3 eV (Mo^{6+}) and 231.4 eV (Mo^{5+}) revealed that the amount of reduced molybdenum was always smaller than 10%. The Mo/Bi ratio had no detectable influence on the reducibility of the Bi species. Interestingly, no change in the surface Bi/Mo/Ti ratio of the sol–gel mixed oxides could be observed during the reduction process, but the missing effect may also be due to the limited sensitivity of XPS.

These observations reveal that Bi^{3+} in sol–gel derived bismuth molybdenum titanium mixed oxides can be easily reduced to Bi^0 and re-oxidized to Bi^{3+} at room temperature. Another interesting feature of these materials

is that Bi^{3+} could be reduced in a much larger extent than Mo^{6+}. In contrast, Grzybowska *et al.* (5) and Uchida *et al.* (7) found that the reduction and re-oxidation of Mo^{6+} was more facile than that of Bi^{3+} in conventional bismuth molybdates.

Stability of Surface Bi^{3+} and Mo^{6+} Species in γ-Bi_2MoO_6 and Bi_2O_3

In order to reveal the influence of the sol–gel technique and the surface redox properties of the mixed oxides, we extended our study to the crystalline γ-Bi_2MoO_6 and Bi_2O_3. γ-Bi_2MoO_6 was chosen as reference material because it represents the most investigated bismuth molybdate in the literature (5–7). After evacuation in the load lock for a prolonged time period (up to 48 h), we could not detect any reduced species on the surfaces of γ-Bi_2MoO_6 and Bi_2O_3, which is in accordance with former observations (5–7, 23).

It was assumed that organic residues originating from the sol–gel preparation might influence the redox behavior of Bi^{3+}. Hence, we treated the conventional γ-Bi_2MoO_6 with acetone and ethanol before evacuation. Although this treatment resulted in a significantly higher (surface) carbon content, the redox properties of the sample did not change.

Similarly, after treatment in a hydrogen atmosphere at 10^{-4} mbar for several hours at ambient temperatures, no reduced bismuth or molybdenum species could be detected, in agreement with previous studies (5–7). Reduction of Bi^{3+} occurred only after heating the γ-Bi_2MoO_6 up to elevated temperatures: ca 13% at 573 K and 16% at 800 K. A similar behavior was reported by Grzybowska *et al.* (5) who found some reduction of Bi^{3+} after exposing γ-bismuth molybdate to hydrogen for 10 min at 743 K. Further reduction during 1 h resulted in a significantly reduced surface. Moreover, Uchida *et al.* have reported on the activation energies for re-oxidation of Mo^{5+} and Bi^0 of α- and γ-bismuth molybdate finding that the activation energies are lower for the γ-phase. However, we cannot confirm that Mo^{6+} is more easily reduced to Mo^{5+} than Bi^{3+} to Bi^0 as was reported by the above authors. Applying 10^{-4} mbar hydrogen we found only a small shoulder at 231.4 eV (<5%) which could be attributed to Mo^{5+} as it can be seen in Fig. 3, but we did not see Mo^{4+} species at 228.3 eV as it was reported by Grzybowska *et al.* after reduction in hydrogen at 1 bar. Reoxidation of our slightly reduced sample or further reduction of the samples could not be performed at room temperature. These observations suggest that in the sol–gel derived materials bismuth possesses a unique reduction–oxidation behavior.

Bulk Reduction of Sol–Gel Bismuth Molybdenum Titanium Mixed Oxides

Temperature programmed reduction (TPR) with the freshly calcined samples 10BiMoTiO-LT, 10BiMoTiO-XClP and 10BiMoTiO-XCl was carried out in order to reveal if the reduction in the XPS chamber was limited to the surface layer of the catalyst or if the bulk of the mixed oxide also took part in the redox process at ambient temperature. The experiments were carried out starting at room temperature. No H_2 consumption was observed below 450 K, indicating that reduction of the bulk is unlikely.

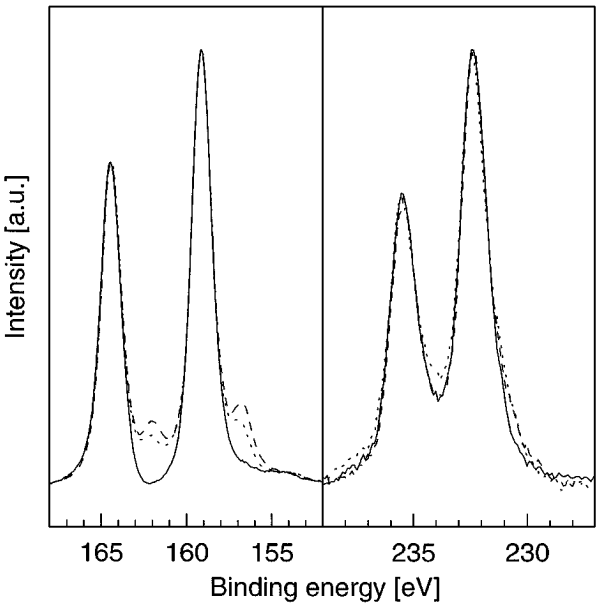

FIG. 3. XP-spectra of γ-Bi_2MoO_6 in the Bi 4f and in the Mo 3d regions. Original spectrum at room temperature (solid line), after reduction in 10^{-4} mbar H_2 at 573 K (dotted line), and after reduction in 10^{-4} mbar H_2 at 800 K (dashed line). The binding energy values are given in Table 3.

To study the beginning reduction of the bulk in more detail, pulse thermal analysis (PTA) with the 10BiMoTiO-LT was carried out. In order to minimize the disturbing effect of physisorbed water, the catalyst was heated to 373 K (in argon). Despite of the high sensitivity of PTA, no weight loss due to reduction of the bulk could be detected by H_2 pulses, and monitoring the evolving gases did not show any H_2 consumption. An increase of the temperature in steps of 100 K showed that the reduction started between 673 and 773 K. Also these results indicate that only the outer surface layer of the sol–gel materials could be reduced at room temperature. Moreover, the amount of reducible surface layer(s) seems to be rather small compared to the total amount of bismuth molybdate in the catalyst.

Time-Resolved Surface Reduction and Re-oxidation at Ambient Temperature

As shown before, most of the sol–gel derived samples could be easily reduced and re-oxidized at room temperature. We investigated the redox behavior of one catalyst, the 10BiMoTiO-LT aerogel, in greater detail by reacting it with hydrogen and oxygen. The time-resolved redox behavior of the surface could be followed quasi *in situ* by performing the

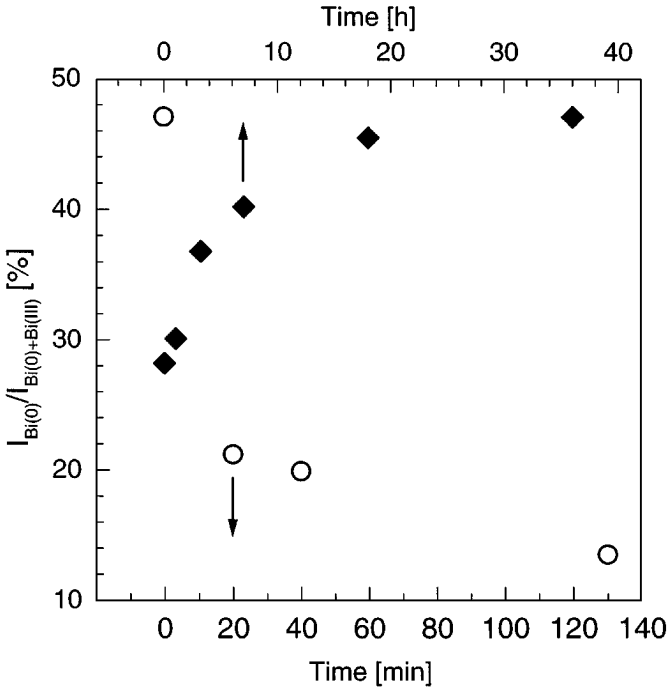

FIG. 4. Amount of surface Bi present as Bi^0 (percentage of Bi^0-intensity in XPS) of 10BiMoTiO-LT during reduction in 10^{-6} mbar H_2 (◆, top axis) and during re-oxidation in 10^{-4} mbar O_2 (○, bottom axis).

reduction/re-oxidation in the reactor chamber and analysis in the XPS chamber. It was shown above that the reaction could be stopped under UHV conditions and the oxidation state of the aerogel was not affected by X-ray radiation. A typical cycle of the reduction of the 10BiMoTiO-LT aerogel (at a partial pressure of 10^{-6} mbar H_2) and re-oxidation (at a partial pressure of 10^{-4} mbar O_2) is shown in Fig. 4. In both cases, the rate of the surface redox process was very fast at the beginning, followed by a slower increase of Bi^0 intensity (reduction) and Bi^{3+} intensity (oxidation), respectively. The decline and the growth of the reduced surface layer was not finished even after 2 h (in oxygen) or 40 h (in hydrogen), respectively. The slow completion of the process can be explained as follows: Underlying layers are detected as well in XPS due to the mean free path of the electrons in the substrate between 0.5 and 3 nm (in the energy range 20–1500 eV (25)). However, the deeper the considered layer, the smaller is the contribution of its atoms to the signal intensity in XPS. Furthermore, the reduction/oxidation rate on the surface seems to differ from the one in the bulk. A continuous oxide film may grow on the surface which could hinder the transport of the reactants to the metal atoms (26, 27).

It was also found that the reaction rates were strongly dependent on the partial pressures in the range of 10^{-4} to 10^{-6} mbar. Further investigations aiming at revealing the mechanism of the reduction–oxidation process is currently performed in our laboratory.

4. DISCUSSION

The results reported in this study show that bismuth molybdenum titanium mixed oxides, prepared via different sol–gel techniques, exhibit altered properties as compared to conventional bismuth molybdate catalysts. Especially, we observed that Bi^{3+} in sol–gel derived bismuth molybdenum titanium mixed oxides can be easily reduced to Bi^0 and re-oxidized to Bi^{3+} at room temperature. In contrast, Bi^{3+} of γ-Bi_2MoO_6 and Bi_2O_3 did not possess such surface redox properties.

The comparison of various sol–gel xerogels and an aerogel showed that the bulk or surface compositions as well as the nature of precursors and the drying method did not influence the surface redox behavior markedly. Nonetheless, the 10BiMoTiO-XClP xerogel prepared by prehydrolysis was not reducible at all at room temperature, revealing that careful prehydrolysis of $MoOCl_4$ and $BiCl_3$ precursors can provide a bismuth molybdenum oxide phase which is stable against reduction.

The ease of reduction of the surface seems to be linked mainly to the morphological and structural properties of the sol–gel samples. Indeed, the Bi- and Mo-containing phases were amorphous in XRD and Raman studies. These phases are excellently stabilized by the titania matrix of the mixed oxides, even after calcination at elevated temperatures.

Since thermoanalysis revealed that bulk reduction is not observed even at 373 K in hydrogen, we can conclude that the amount of reducible bismuth is negligible compared to the total bismuth content of the catalysts. Hence, the particles themselves are rather large and might be composed of small agglomerated crystalline regions. Taking into account the sensitivity of the pulse analytical methods, we propose that the average particle size should be markedly higher (>10 nm) than the size of the Bi-containing crystallites (ca 3 nm) estimated by XRD. γ-Bismuth molybdate, which did not exhibit such a reduction–oxidation behavior on the surface at ambient temperature, was composed of crystallites with a 210-nm average diameter. The facile reduction and re-oxidation of the bismuth molybdenum titanium mixed oxides might therefore be attributed to an increased activity of the lattice oxygen because of the small size of bismuth molybdate crystallites. Similar observations were made recently by Soares *et al.* (28) who reported that surface reduction was more pronounced for sol–gel derived than for coprecipitated iron molybdate catalysts. To our knowledge, such a smooth reduction and re-oxidation of Bi^{3+} has not yet been observed at room temperature for bismuth oxide or Bi-containing mixed oxides.

5. CONCLUSIONS

XPS surface analysis combined with treatment of the sample with hydrogen or oxygen in an adjacent reactor

chamber was demonstrated to be a useful tool to investigate the surface redox behavior of bismuth molybdenum oxides. The pressure- and temperature-dependent oxidation and reduction cycles of the material surface could be studied quasi *in situ* at varying pressures (10^{-6}–10^{-4} mbar).

Up to now, there are only a few reports on systems which show such a redox behavior at ambient temperature, e.g. in corrosion science, where oxidation of metals was studied at low oxygen pressures with XPS (27). However, to our knowledge, no XPS study on thin films and powders was reported with a reversible reduction–oxidation behavior at room temperature. Our observations confirm that sol–gel preparation techniques can result in materials with altered structural properties. These results provide a good starting point to investigate the catalytic performance of the sol–gel derived mixed oxides. It seems to be important to choose a reaction which requires mild conditions. At elevated temperatures the unique properties of Bi-Mo-Ti mixed oxides can be partly or fully lost due to restructuring, as has been observed in the oxidation of butadiene to furan (29).

ACKNOWLEDGMENTS

Thanks are due to M. Maciejewsky for the XRD and thermoanalytical measurements and to C. A. Müller for the preparation of the aerogel. Financial support by Du Pont de Nemours, Wilmington, DE, is kindly acknowledged.

REFERENCES

1. Sant, B. R., Rao, S. B., Rao, J. R., Thakur, R. S., and Parida, K. M., *J. Sci. Ind. Res.* **43**, 542 (1984).
2. Grasselli, R. K., *in* "Handbook of Heterogeneous Catalysis" (G. Ertl, H. Knözinger, and J. Weitkamp, Eds.), Vol. 5, p. 2302. Wiley-VCH, Weinheim, 1997.
3. Moro-Oka, Y., and Ueda, W., *Adv. Catal.* **40**, 233 (1994).
4. Brazdil, J. F., Suresh, D. D., and Grasselli, R. K., *J. Catal.* **66**, 347 (1980).
5. Grzybowska, B., Haber, J., Marczewski, W., and Ungier, L., *J. Catal.* **42**, 327 (1976).
6. Matsuura, I., Schut, R., and Hirakawa, K., *J. Catal.* **63**, 152 (1980).
7. Uchida, K., and Ayame, A., *Surf. Sci.* **357–358**, 170 (1996).
8. Arora, N., Deo, G., Wachs, I. E., and Hirt, A. M., *J. Catal.* **159**, 1 (1996).
9. Schneider, M., and Baiker, A., *Catal. Rev.-Sci. Eng.* **37**, 515 (1995).
10. Wildberger, M. D., Grunwaldt, J.-D., Mallat, T., and Baiker, A., *Appl. Catal. A*, submitted.
11. "JCPDS Mineral Powder Diffraction Data Files," Park Lane, Pennsylvania.
12. Koeppel, R. A., Nickl, J., and Baiker, A., *Catal. Today* **20**, 45 (1994).
13. Shirley, D. A., *Phys. Rev. B* **5**, 4709 (1972).
14. Briggs, D., and Seah, M. P., "Practical Surface Analysis by Auger and X-ray Photoelectron Spectroscopy," Wiley, Chichester, 1983.
15. Stencel, J. M., "Raman Spectroscopy for Catalysts," Vol. 2, Van Nostrand Reinhold, New York, 1990.
16. Lin, Z. M., and Vannice, M. A., *Surf. Sci.* **350**, 45 (1996).
17. Grunwaldt, J. D., Göbel, U., and Baiker, A., *Fresenius J. Anal. Chem.* **358**, 96 (1997).
18. Firment, L. E., and Ferretti, A., *Surf. Sci.* **129**, 155 (1983).
19. Haber, J., and Lalik, E., *Catal. Today* **33**, 119 (1997).
20. Notermann, T., Keulks, G. W., Skiliarov, A., Maximov, Y., Margolis, L. Y., and Krylov, O. V., *J. Catal.* **39**, 286 (1975).
21. McGilp, J. Y., Weightmar, P., and McGuire, E. Y., *J. Phys. C: Solid State Phys.* **10**, 3445 (1977).
22. Dharmadhikari, V. S., Sainkar, S. R., Badrinarayan, S., and Goswami, A., *J. Electron Spectrosc. Relat. Phenom.* **25**, 181 (1982).
23. Shuk, P., Wiemhöfer, H.-D., Guth, U., Göpel, W., and Greenblatt, M., *Sol. State Ionics* **89**, 179 (1996).
24. Fung, K. Z., and Virkar, A. V., *J. Am. Chem. Soc.* **74**, 1970 (1991).
25. Seah, M. P., and Dench, W. A., *Surf. Interf. Anal.* **1**, 2 (1979).
26. Lawless, K. R., *Rep. Prog. Phys.* **37**, 232 (1974).
27. Fehlner, F. P., "Low-Temperature Oxidation: The Role of Vitreous Oxides," Wiley, Pennington, 1981.
28. Soares, A. P. V., Portela, M. F., and Kiennemann, A., *in* "Proc. 3rd World Congress on Oxidation Catalysis, San Diego, 1997" (R. K. Grasselli, S. T. Oyama, A. M. Gaffney, and J. E. Lyons, Eds.), p. 807. Elsevier Science, Amsterdam. 1997.
29. Wildberger, M. D., Maciejewski, M., Grunwaldt, J.-D., Mallat, T., and Baiker, A., *J. Catal.*, submitted.